RESEARCH ARTICLE

WILEY

The trajectory of the medial longitudinal fasciculus in the human brain: A diffusion imaging-based tractography study

Mengjun Li[1] | Fang-Cheng Yeh[2,3] | Qingrun Zeng[4,5] | Xiaolong Wu[1] |
Xu Wang[1] | Zixin Zhu[1] | Xiaohai Liu[1] | Jiantao Liang[1] | Ge Chen[1] |
Hongqi Zhang[1] | Yuanjing Feng[4,5] | Mingchu Li[1]

[1]Department of Neurosurgery, Capital Medical University Xuanwu Hospital, Beijing, China

[2]Department of Neurological Surgery, University of Pittsburgh School of Medicine, Pittsburgh, Pennsylvania, USA

[3]Department of Bioengineering, University of Pittsburgh School of Medicine, Pittsburgh, Pennsylvania, USA

[4]Institute of Information Processing and Automation, College of Information Engineering, Zhejiang University of Technology, Hangzhou, China

[5]Zhejiang Provincial United Key Laboratory of Embedded Systems, Hangzhou, China

Correspondence
Mingchu Li, Department of Neurosurgery, Capital Medical University Xuanwu Hospital, Samii's Clinical Neuroanatomy Research & Education Center, China International Neuroscience Institute (China-INI), Beijing, China.
Email: mingchu_li@xwhosp.org

Abstract

The aim of this study is to investigate the trajectory of medial longitudinal fasciculus (MLF) and explore its anatomical relationship with the oculomotor nerve using tractography technique. The MLF and oculomotor nerve were reconstructed at the same time with preset three region of interests (ROIs): one set at the area of rostral midbrain, one placed on the MLF area at the upper pons, and one placed at the cisternal part of the oculomotor nerve. This mapping protocol was tested in an HCP-1065 template, 35 health subjects from Massachusetts General Hospital (MGH), 20 healthy adults and 6 brainstem cavernous malformation (BCM) patients with generalized q-sampling imaging (GQI)-based tractography. Finally, the 200 μm brainstem template from Center for In Vivo Microscopy, Duke University (Duke CIVM), was used to validate the trajectory of reconstructed MLF. The MLF and oculomotor nerve were reconstructed in the HCP-1065 template, 35 MGH health subjects, 20 healthy adults and 6 BCM patients. The MLF was in conjunction with the ipsilateral mesencephalic part of the oculomotor nerve. The displacement of MLF was identified in all BCM patients. Decreased QA, RDI and FA were found in the MLF of lesion side, indicating axonal loss and/or edema of displaced MLF. The reconstructed MLF in Duke CIVM brainstem 200 μm template corresponded well with histological anatomy. The MLF and oculomotor nerve were visualized accurately with our protocol using GQI-based fiber tracking. This GQI-based tractography is an important tool in the reconstruction and evaluation of MLF.

KEYWORDS
generalized Q-sampling imaging, medial longitudinal fasciculus, oculomotor nerve, tractography

1 | INTRODUCTION

The medial longitudinal fasciculus (MLF) is a highly specialized and organized fiber bundle composed of ascending and descending white matter tracts. The majority of its fiber tracts come from the vestibular nucleus and the nuclei of extraocular muscles (nucleus of oculomotor nerve, nucleus of trochlear nerve and nucleus of abducens nerve), some fiber tracts arise from the Darkschewitsch nucleus, the

interstitial nucleus of Cajal and the rostral interstitial nucleus of the MLF. The ascending fiber tracts, mostly originating from the vestibular nucleus and the abducens nucleus, travel to the oculomotor nerve nucleus, the trochlear nerve nucleus, the interstitial nucleus of Cajal and the rostral interstitial nucleus of the MLF. The descending fiber tracts, mainly arising from the vestibular nucleus and interstitial nucleus of Cajal, project to the intermediate zone and the medial nucleus of the anterior horn of the cervical spinal cord (Nieuwenhuys, Voogd, & van Huijzen, 1988). The MLF ascending and descending fiber tracts travel together in a dorsomedial direction throughout the brainstem. First, the MLF starts from the interstitial nucleus of Cajal and the rostral interstitial nucleus of the MLF and runs ventrolateral to the cerebral aqueduct in front of the nucleus of oculomotor nerve at the rostral midbrain. Then, it travels ventral to the fourth ventricle floor and lateral to the median sulcus in front of the dorsal longitudinal fasciculus at the pons. Finally, the MLF courses ventral to the central gray matter in the medulla and projects caudally into the anterior funiculus of the spinal cord.

Functionally, the MLF plays a key role in the adjustment of coordinated and synchronized eye movements based on the connection within the nucleus of extraocular muscles (McNulty et al., 2016; Sakai, Yokota, Akazawa, & Yamada, 2014; Yeo, Jang, Kwon, & Cho, 2020). Furthermore, it takes part in conjugate eye movements, including saccadic eye movements and smooth pursuit (Frohman et al., 2008). In addition, the MLF is essential for the vestibulo-ocular reflex, which can stabilize the retinal images by producing eye movements compensatory for head movements (Nieuwenhuys et al., 1988), and the vestibular-ocular fibers in the MLF are also in charge of coordination balance and linear acceleration through the semicircular and otolith-mediated oculomotor reflex (Bae, Kim, Choi, Jung, & Kim, 2013; Fiester, Baig, Patel, & Rao, 2020).

The specific clinical signs produced by MLF injury can be divided into four distinct categories of disease based on the affected anatomy and function: (1) internuclear ophthalmoplegia (INO), (2) INO and trochlear syndrome, (3) INO and one-and-a-half syndrome, and (4) wall-eyed bilateral INO syndrome (Fiester et al., 2020). To investigate the correlation between MLF injury and clinical manifestations, diffusion tensor imaging (DTI) was used to evaluate the integrity of this fiber bundle through DTI metrics. The mean diffusivity (MD) in the MLF was found to correlate with the velocity versional disconjugacy index in multiple sclerosis patients (Fox et al., 2008), and the longitudinal diffusivity and fractional anisotropy (FA) of the MLF were lower in the multiple sclerosis patients than in healthy controls. Longitudinal diffusivity and FA were also correlated with the velocity disconjugacy index (Sakaie et al., 2016). However, these DTI studies did not reconstruct the fiber pathways of the MLF, and only one study visualized the trajectory of the MLF in healthy controls with DTI techniques (Yeo et al., 2020). On the other hand, traditional DTI-based fiber tracking cannot resolve the crossing fibers that result from the simple 1-fiber model for each voxel, and these limitations were also encountered in the analysis of fiber tracts in the tumor edema zone (Fernandez-Miranda et al., 2012; Zhang et al., 2013). Furthermore, the indices of DTI suffered from partial volume effects (Yeh, Verstynen, Wang, Fernández-Miranda, &

Tseng, 2013), which were more obvious in the brainstem since this vital structure is structurally compact and contains various nucleus and fibers. To overcome these limitations, advanced diffusion MRI has been applied to visualize this fiber bundle. The MLF was visualized originating from the rostral midbrain, running dorsally in the mesencephalic tegmentum and descending dorsally to the decussation of the superior cerebellum peduncle in a template reconstructed from the Human Connectome Project (HCP) subjects (Meola, Yeh, Fellows-Mayle, Weed, & Fernandez-Miranda, 2016). Moreover, the MLF was identified in the fiber dissection study, which found that the MLF is in conjunction with the mesencephalic part of the oculomotor nerve in the midbrain (Yagmurlu, Rhoton Jr., Tanriover, & Bennett, 2014). At the same time, the MLF was found to continue with the mesencephalic part of the oculomotor nerve in the midbrain using high-definition fiber tractography in 5 healthy subjects (Yoshino et al., 2016). However, there is still no study to map MLF in brainstem cavernous malformations (BCM) patients using diffusion MRI tractography currently.

In this study, we aimed to thoroughly investigate the trajectory of the MLF and explore its anatomic relationship with oculomotor nerve using high definition fiber-tracking tractography. We attempted to track the MLF through diffusion spectrum imaging (DSI) reconstructed by generalized q-sampling imaging (GQI) tractography using both subject-specific and template approaches (Yeh, Wedeen, & Tseng, 2010). This approach has reconstructed the MLF successfully and provided accurate fiber tractography in known complex neuroanatomical features and tumors surrounding edema zones (Celtikci, Fernandes-Cabral, Yeh, Panesar, & Fernandez-Miranda, 2018; Panesar, Belo, Yeh, & Fernandez-Miranda, 2019), and our group has visualized the subcomponents of the ansa peduncularis with this high-angular resolution approach (Li et al., 2020). High-definition fiber tractography has also been demonstrated to have the ability to accurately define the relationship between the brainstem cavernous malformations (BCM) and perilesional displaced and/or disrupted white matter (Faraji et al., 2015). This study will better our understanding of the MLF connectivity in the human brain.

2 | METHODS

In our work, we reconstructed the MLF in an HCP-1065 template, 35 healthy subjects from Massachusetts General Hospital (MGH), 20 healthy adults and six BCM patients whose lesions were located next to the MLF from Xuanwu Hospital. Then, DTI and GQI metrics were evaluated on both the lesion side and contralateral side to investigate the changes of MLF caused by BCM. Finally, the MLF was visualized in the 200 μm brainstem template from Center for In Vivo Microscopy, Duke University (Duke CIVM), to validate its trajectory with histological anatomy.

3 | PARTICIPANTS

Twenty neurologically healthy adults (12 men and 8 women; age range 22–57 years) and six BCM patients (2 men and 4 women; age

range 27–58 years) were recruited from April 2016 to December 2020. All participants were prescreened prior to scanning to rule out any contraindications to MRI. Approval was granted by the Ethics Committee of Xuanwu Hospital, Capital Medical University. Written informed consent was obtained from all participants before testing.

In addition, we conducted fiber tracking in 35 Massachusetts General Hospital (MGH) healthy adults and in the HCP-1065 template constructed from HCP subjects. The HCP consortium is an ongoing project led by Washington University, the University of Minnesota, and Oxford University, with the goal of mapping connections and functions in the human brain. This template was constructed from a total of 1,065 subjects' diffusion MRI data from the HCP (2017 Q4, 1,200-subject release).

3.1 | Image acquisition

The diffusion data of healthy controls were acquired using a 3.0T Siemens Prisma MRI scanner (Siemens Healthineers, Erlangen, Germany) with a 64-channel head coil and a head stabilizer was used to reduce head motion. A DSI 2D echo-planar imaging sequence was applied with the following parameters: b-values ranging from 275 to 7,015 s/mm^2; 514 diffusion directions; echo time (TE): 97 ms; repetition time (TR): 5,000 ms; and voxel size = 2.2 mm × 2.2 mm × 2.2 mm. The diffusion data of six BCM patients were acquired in a 3.0T Siemens Skyra MRI scanner (Siemens Healthineers, Erlangen, Germany) with the following parameters: b-value was 1000s/mm^2; TR:8900 ms; TE:95 ms; the number of diffusion sampling directions was 64; and voxel size = 2.2 mm × 2.2 mm × 2.2 mm. To achieve high-resolution anatomical comparisons, a T1 magnetization-prepared rapid gradient echo sequence was performed with the following parameters: TR: 2400 ms; TE: 2.7 ms; flip angle = 8°; and voxel size = 1.0 mm × 1.0 mm × 1.0 mm. All subjects were confirmed to have minimal head movement during scanning. Movement corrections and eddy current corrections were preprocessed in the FSL (Jenkinson, Beckmann, Behrens, Woolrich, & Smith, 2012). Then, the preprocessed diffusion data were analyzed by DSI studio (http://dsi-studio.labsolver.org/). The GQI was used to reconstruct the orientation-distribution function (ODF) map. The diffusion sampling length ratio was 1.1 with ODF sharpening off (Yeh et al., 2010).

3.2 | The HCP MGH data and HCP-1065 template

Thirty-five MGH healthy adult diffusion data from the HCP were used to reconstruct the MLF. The b-values of the diffusion data were 1,000, 3,000, 5,000 and 9,950 s/mm^2, and the corresponding number of diffusion sampling directions was 64, 64, 128, and 256, respectively. The in-plane resolution was 1.5 mm, which was the same as the slice thickness. These data are freely available for download at https://db.humanconnectome.org.

Additionally, a total of 1,065 subjects' diffusion MRI data from the HCP was used to reconstruct the HCP-1065 template. The b-

values of the diffusion data were 1,000, 2,000 and 3,000 s/mm^2, and the corresponding number of diffusion sampling directions was 90, 90, and 90, respectively. The in-plane resolution was 1.25 mm, which was the same as the slice thickness. The diffusion data of each subject were registered and reconstructed into the ICBM-152 space to obtain the spin distribution function by the q-space diffeomorphic reconstruction. Then the spin distribution function of all subjects was averaged voxel by voxel to obtain the HCP-1065 template (Yeh et al., 2018; Yeh & Tseng, 2011). The reconstruction was conducted in the DSI Studio. The resolution of the template applied in our study was 1 mm. This template is downloadable at http://dsi-studio.labsolver.org/download-images.

3.3 | The Duke CIVM brainstem 200 μm template

The Duke CIVM Brainstem 200 μm template was used to reconstruct the MLF and validate its trajectory with histological anatomy. This brainstem template was constructed based on a specimen extending from the rostral diencephalon to the caudal medulla through magnetic resonance histology, and provided anatomic and diffusion atlas to visualize and analysis the microscopic anatomy of the brainstem with rendered isotropic resolution of 200 μm (Adil et al., 2021; Calabrese et al., 2015). The specimen was scanned in a 7-Tesla MRI scanner to acquire the anatomic and diffusion images. The b-value of the diffusion data was 4,000 s/mm^2 and the diffusion sampling directions was 120. The in-plane resolution was 0.2 mm, which was the same as the slice thickness. The GQI was used to reconstruct the diffusion data and the diffusion sampling length ratio was 0.4 (Yeh et al., 2010). This template is downloadable at https://civmvoxport.vm.duke.edu/voxbase/login.php?return_url=%2Fvoxbase%2F.

3.4 | Fiber tracking

All fiber tracking was performed using DSI Studio. The tracks were visualized by preset region of interest (ROIs) based on the ODF and T1 image (Figure 1). The left MLF and left oculomotor nerve were tracked at the same time with preset three ROIs: one ROI set at the area of rostral midbrain, one was placed on the MLF area at the level of the upper pons in front of the fourth ventricle floor and one ROI was placed at the left cisternal part of the oculomotor nerve. The right MLF and right oculomotor nerve were also tracked at the same time with preset three ROIs, but changing the third ROI for right side (placed at the right cisternal part of the oculomotor nerve). In order to exclude the dorsal longitudinal fasciculus (DLF), which has a close trajectory to the MLF but end in the hypothalamus, one region of avoidance (ROA) has been placed at the hypothalamus to exclude the DLF. With these ROIs and ROA, both the oculomotor nerve and MLF can be tracked successfully at the same time (Meola et al., 2016; Yeo et al., 2020; Yoshino et al., 2016), and the MLF will be determined accurately according to the conjunction with the mesencephalic part of the oculomotor nerve.
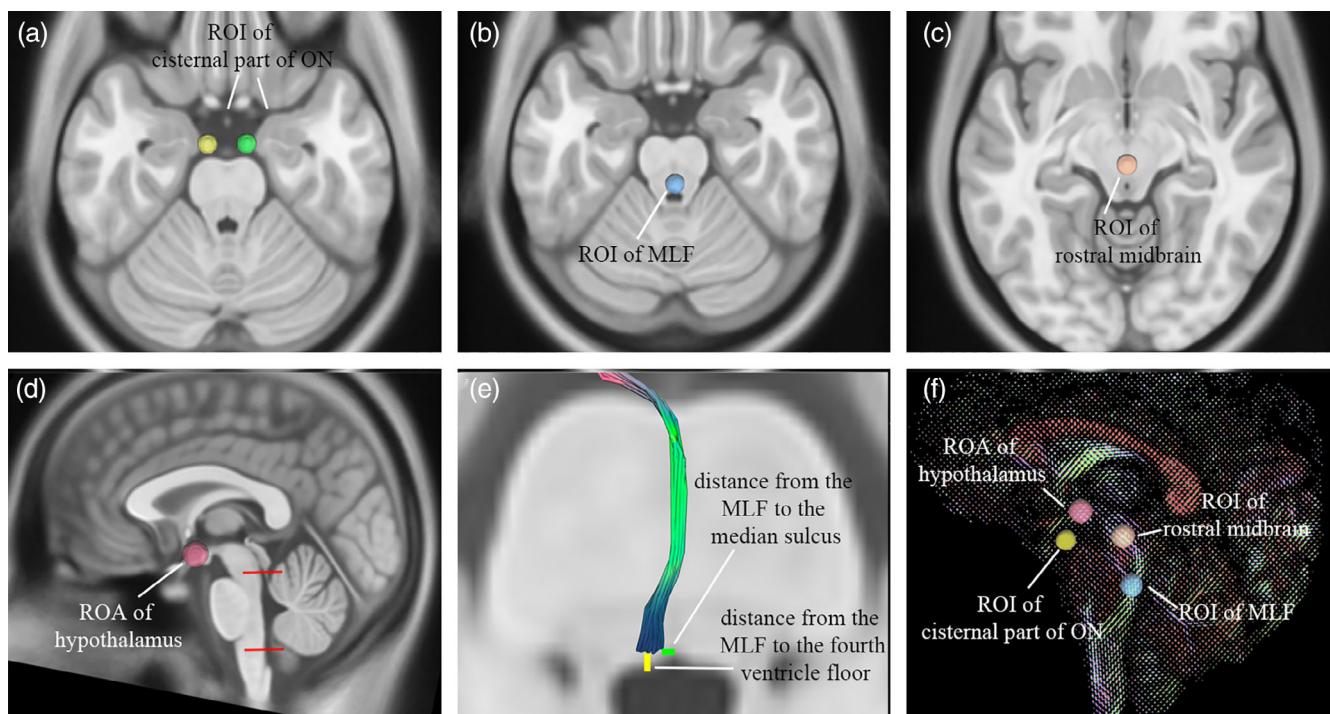
FIGURE 1 In vivo fiber tractography of the MLF: ROI placement. (a) The ROI of the left (yellow) and right (green) cisternal part of the oculomotor nerve. (b) The ROI (blue) of MLF at the level of the upper pons in front of the fourth ventricle floor. (c) The ROI (orange) of MLF at the rostral midbrain. (d) The ROA (red) of MLF at the hypothalamus. The upper red line was the beginning level at which the distances from the MLF to the median sulcus and to the fourth ventricle floor were measured. The red line below was the ending level at which the distances from the MLF to the median sulcus and to the fourth ventricle floor were measured. (e) The distances from the MLF to the fourth ventricle floor (yellow line) and to the median sulcus (green line) were measured. (f) The left MLF ROIs and ROA overlaid on the ODF sagittal slice. ON, oculomotor nerve

In voxels with multiple fiber orientations, fiber tracking was initiated separately for each orientation, and fiber progression continued with a step size of 0–1.2 mm, a minimum fiber length of 30 mm, and a turning angle threshold of 60°–90°. To smooth each track, the next moving directional estimate of each voxel was weighted by 20% of the previous incoming direction and 80% of the nearest fiber orientation. This progression was repeated until the quantitative anisotropy (QA) of the fiber orientation dropped below a preset threshold. Once tracked, all streamlines were saved in the TrackVis file format (Fernández-Miranda et al., 2015; Li et al., 2020). This deterministic fiber tracking method in DSI Studio was shown to achieved the highest rate of valid connections (92%) out of 96 methods submitted from 20 different groups, as examined by open competition, the average accuracy was 54% (Maierhein et al., 2017).

3.5 | Data analysis

In the HCP template tractography, the lengths and diameters of the MLF and oculomotor nerve were measured. In addition, the distances from the MLF to the fourth ventricle floor and to the median sulcus were measured (Figure 1). In the subject-specific tractography, the QA, RDI (restricted diffusion imaging), FA, axial diffusivity (AD) and MD value of the MLF in the MGH subjects and healthy controls were compared between the left and right sides of the brainstem with the paired-sample t test in SPSS 22.0. Continuous variables are presented as the mean ± SD. For BCM patients whose lesions were located next to the MLF and caused corresponding clinical presentations, qualitative analysis was used to evaluate the displacement and/or disruption of the MLF in the lesion side through comparisons with the contralateral homologous MLF. Displacement was defined as a change in location or direction of the affected MLF due to the BCM mass effect. Disruption was defined as thinning of the affected MLF, discontinuity in part of the affected MLF or lack of visualization in most or all of its anatomy course. Then, quantitative analysis was carried out to validate the previous qualitative changes, paired-sample t tests were adopted to determine variances in QA, RDI, FA, AD, and MD values of the MLF between the lesion side and contralateral side. $p \leq .05$ was considered to be statistically significant.

4 | RESULTS

4.1 | HCP-1065 template tractography results

The cisternal part of the oculomotor nerve, the mesencephalic part of the oculomotor nerve and MLF were tracked in the HCP-1065 template. The rostral part of the left MLF was in conjunction with the

ipsilateral mesencephalic part of the oculomotor nerve at the level of the superior colliculus in front of the nucleus of the oculomotor nerve. The rostral part of the right MLF was in conjunction with the ipsilateral mesencephalic part of the oculomotor nerve at the level of the superior colliculus in front of the nucleus of the oculomotor nerve. Then, both the left and right MLF descended ventrolateral to the cerebral aqueduct and dorsal to the decussation of superior cerebellum peduncle at the midbrain. After that, the MLF traveled ventral to the fourth ventricle floor and lateral to the median sulcus in the pons. Finally, the caudal part of the MLF descended ventral to the central gray matter in the medulla and terminated superior to the gracile tubercle due to the fiber tracking reached the template bottom.

In addition, the lengths and diameters of the MLF and oculomotor nerve and the distances from the MLF to the fourth ventricle floor and to the median sulcus were measured. The lengths of the oculomotor nerve were 36.3 mm and 35.6 mm in the left and right sides of the brainstem, respectively, the lengths of the MLF were 43.4 mm and 40.0 mm in the left and right sides of the brainstem, respectively, the

mean diameters of the oculomotor nerve were 2.44 mm and 2.40 mm in the left and right sides of the brainstem, respectively, the mean diameters of the MLF were 2.60 mm and 2.16 mm in the left and right sides of the brainstem, respectively. Moreover, the mean distances from the MLF to the median sulcus at the same axial level were 0.50 ± 0.06 mm and 0.48 ± 0.05 mm in the left and right sides of the brainstem, respectively, the mean distances from the MLF to the fourth ventricle floor at the same axial level were 1.41 ± 0.65 mm and 1.51 ± 0.81 mm in the left and right sides of the brainstem, respectively (Table 1 and Figure 2).

4.2 | Subject-specific tractography results

In 35 MGH cases, the cisternal part of the oculomotor nerve, the mesencephalic part of the oculomotor nerve and MLF were traced in 69 cases (69/70, not identified in 1 case: left side of subject 15). In 20 healthy controls, the cisternal part of the oculomotor nerve, the

TABLE 1 The distances from the MLF to the median sulcus and fourth ventricle floor

Slicer Number	Distance from MLF to the median sulcus (mm)		Distance from MLF to the fourth ventricle floor (mm)	
	L	R	L	R
1	0.58	0.56	3.32	3.86
2	0.47	0.43	2.89	3.53
3	0.53	0.54	2.78	2.99
4	0.54	0.58	1.93	2.25
5	0.53	0.53	1.71	2.03
6	0.43	0.47	1.71	1.71
7	0.42	0.48	1.50	1.61
8	0.42	0.48	1.29	1.30
9	0.43	0.48	1.18	1.29
10	0.42	0.43	1.18	1.17
11	0.43	0.43	1.19	1.17
12	0.42	0.42	1.07	1.07
13	0.48	0.48	1.07	1.07
14	0.48	0.48	1.05	1.01
15	0.48	0.43	1.03	1.01
16	0.48	0.46	1.01	1.01
17	0.48	0.48	1.02	1.03
18	0.54	0.48	1.01	1.03
19	0.52	0.48	1.03	1.03
20	0.52	0.42	1.05	1.07
21	0.58	0.43	1.05	1.07
22	0.58	0.42	1.08	1.09
23	0.55	0.48	1.07	1.1
24	0.58	0.50	1.05	1.05
25	0.53	0.53	1.09	1.1
Mean ± SD	0.50 ± 0.06	0.48 ± 0.05	1.41 ± 0.65	1.51 ± 0.81

Abbreviations: L, left; R, right.
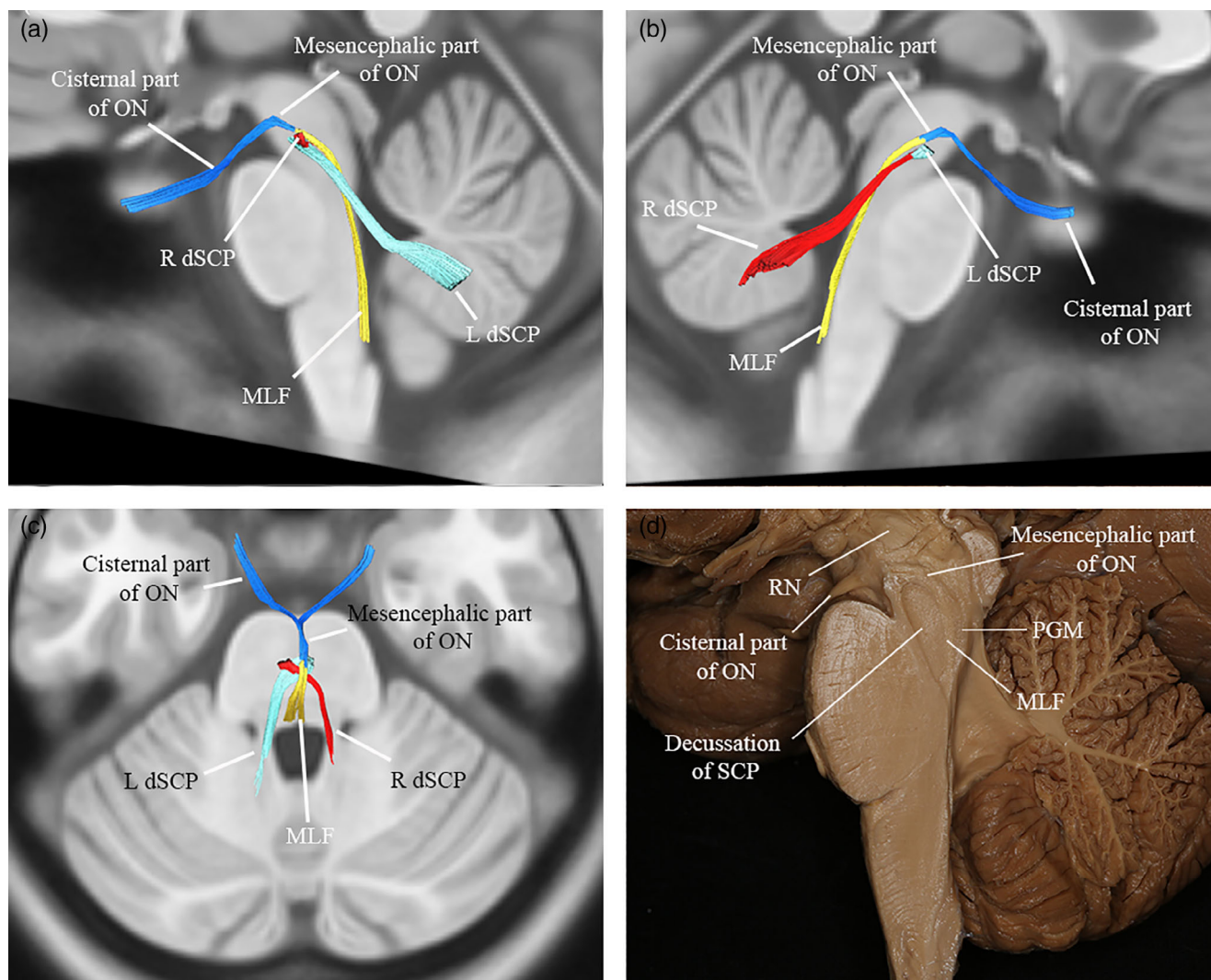
FIGURE 2 The MLF in the HCP-1065 template. (a) Lateral view of the left MLF in the midbrain. (b) Lateral view of the right MLF in the midbrain. (c) Superior view of the left and right MLF in the midbrain. (d) The medial surface of the right hemisphere. The rostral part of the left MLF was in conjunction with the ipsilateral mesencephalic part of the oculomotor nerve at the level of the superior colliculus in front of the nucleus of the oculomotor nerve. The rostral part of the right MLF was in conjunction with the ipsilateral mesencephalic part of the oculomotor nerve at the level of the superior colliculus in front of the nucleus of the oculomotor nerve. Then, both the left and right MLF descended ventrolateral to the cerebral aqueduct and dorsal to the decussation of superior cerebellum peduncle at the midbrain. After that, the MLF traveled ventral to the fourth ventricle floor and lateral to the median sulcus in the pons. Finally, the caudal part of the MLF descended ventral to the central gray matter in the medulla and terminated superior to the gracile tubercle due to the fiber tracking reached the template bottom. dSCP, decussated superior cerebellum peduncle, L, left; ON, oculomotor nerve; PGM, periaqueduct gray matter; R, right; RN, red nucleus; SCP, superior cerebellum peduncle

mesencephalic part of the oculomotor nerve and MLF were reconstructed in 37 cases (37/40, not identified in 3 cases: left side of subject 15, right side of subject 8 and 20). Figure 3 illustrated the trajectory of the MLF in 10 MGH subjects and Figure 4 showed the trajectory of the MLF in 10 healthy controls.

The mean QA, RDI, FA, AD and MD of the MLF in the MGH subjects were 2.92 ± 0.78, 6.35 ± 1.39, 0.13 ± 0.02, 0.24 ± 0.02, and 0.27 ± 0.02 in the left side of the brainstem, respectively, and 2.88 ± 0.84, 6.33 ± 1.39, 0.12 ± 0.02, 0.24 ± 0.02, and 0.28 ± 0.02 in the right side of the brainstem, respectively (Tables 2 and 5). The mean QA, RDI, FA, AD and MD of the MLF in the healthy controls were 0.10 ± 0.05, 0.28 ± 0.15, 0.24 ± 0.12, 0.32 ± 0.21, and 0.44 ± 0.32 in the left side of the brainstem, respectively, and 0.10 ± 0.05, 0.26 ± 0.14, 0.24 ± 0.13, 0.32 ± 0.20, and 0.44 ± 0.30 in the right side of the brainstem, respectively (Tables 3 and 5). A paired-sample t test was used to determine variances in the QA, RDI, FA, AD and MD values between the left and right sides of the brainstem. The AD and MD were significantly different between the left and right MLF in the MGH subjects, while the 20 healthy controls showed no significant differences in the QA, RDI, FA, AD and MD values between the left and right MLF (Table 5).
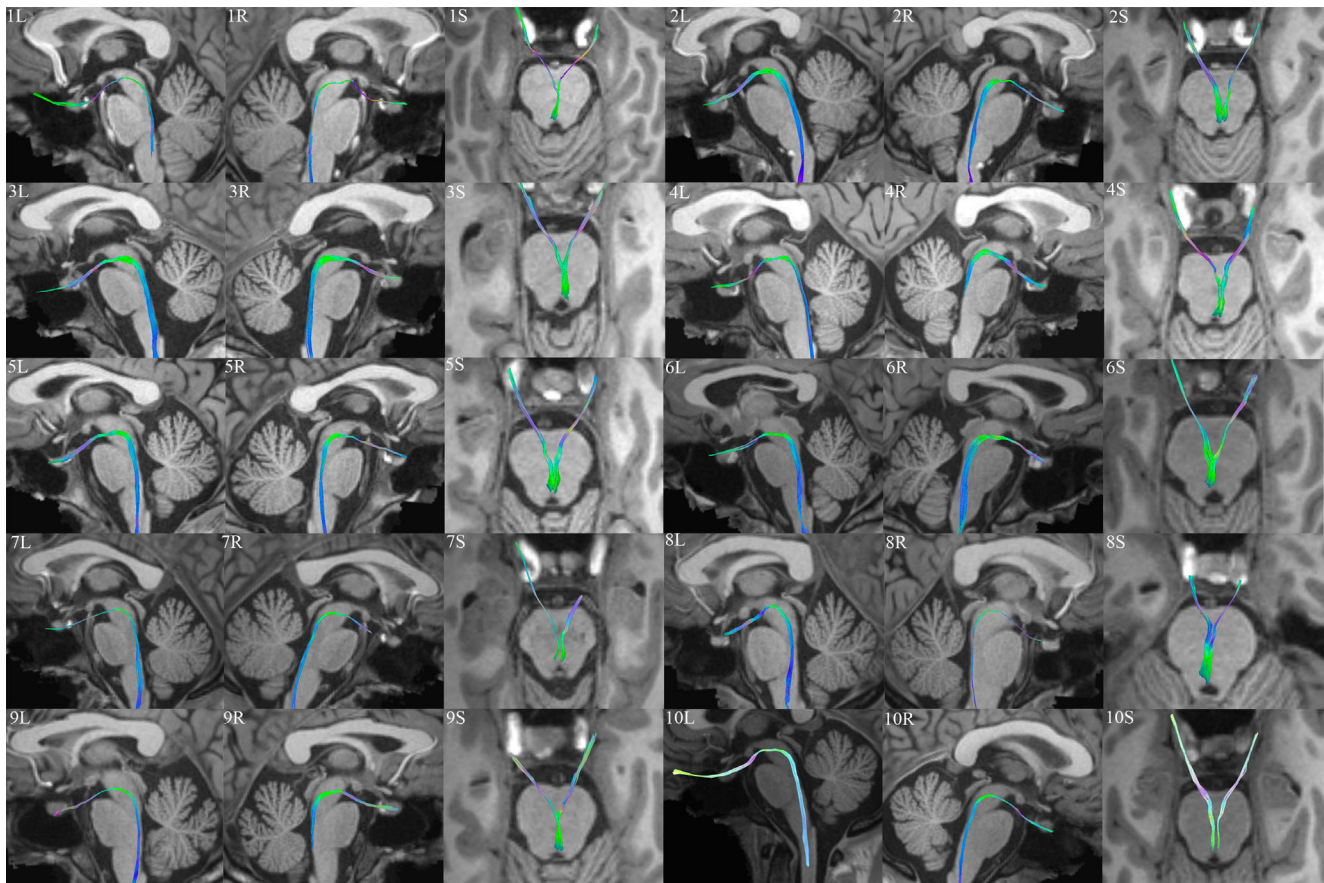
FIGURE 3 Fiber tracking in 10 MGH subjects, showing the lateral view of the left MLF, lateral view of the right MLF and superior view of the left and right MLF. The MLF was traced in 69 cases (left and right). The left MLF was not found in subject 15. L, left; R, right; S, superior

4.3 | BCM tractography results

Qualitative analysis was adopted firstly in 6 BCM patients. The left and right MLF were both displaced by the squeeze of BCM in all BCM patients since these two MLF were adjacent in the brainstem, while disruption was not obvious. In Patient 1, both of the right and left MLF were displaced by the BCM and the right MLF was squeezed to the left side (1S, 1A of Figure 5), this patient had numbness in the left limb but eye movement dysfunction. In Patient 2, both of the right and left MLF were displaced by the BCM and the left MLF was squeezed to the right side, this patient had left facial paralysis but eye movement dysfunction (2S, 2A of Figure 5). In Patient 3, both of the right and left MLF were displaced by the BCM and the right MLF was squeezed to the left side (3S, 3A of Figure 5), this patient had numbness in the left limb combined with horizontal nystagmus. In Patient 4, both of the right and left MLF were displaced by the BCM and the left MLF was squeezed to the right side (4S, 4A of Figure 5), this patient had adduction dysfunction of the left eye. In Patient 5, both of the right and left MLF were displaced inferiorly by the BCM (5S, 5A of Figure 5), this patient had ghosting combined with elevating dysfunction in both eyes. In Patient 6, both of the right and left MLF were displaced by the BCM and the left MLF was squeezed to the right side (6S, 6A of Figure 5), this patient had abduction dysfunction

of the left eye combined with numbness of right limb. The preoperative MLF in relation to the CM was shown in Figure 5.

Quantitative analysis was performed after the qualitative analysis. The mean QA, RDI, FA, AD and MD of the MLF in the BCM patients were 0.062 ± 0.012, 0.088 ± 0.015, 0.36 ± 0.060, 1.62 ± 0.24, and 2.14 ± 0.25 on the lesion side and 0.066 ± 0.011, 0.094 ± 0.014, 0.39 ± 0.068, 1.50 ± 0.32, and 2.02 ± 0.34 on the contralateral side of the brainstem, respectively (Tables 4 and 5). A significant difference was observed in the QA ($p = .012$), RDI ($p = .016$), and FA ($p = .022$) between the lesion side and contralateral side, the QA (decreased 0.0087–11.6%), RDI (decreased 0.74–13.7%) and FA (decreased 1.4–13.2%)value on the lesion side was lower than that on the contralateral side, implying that the MLF of lesion side may have disruption. The MD ($p = .063$) and AD ($p = .113$) value on the contralateral side was lower than that on the lesion side but without significant difference. The demographics and clinical manifestations of the BCM patients were shown in Table 6.

4.4 | Duke CIVM brainstem 200 μm template tractography results

The mesencephalic part of the oculomotor nerve and MLF were tracked in the Duke CIVM brainstem 200 μm template. The trajectory
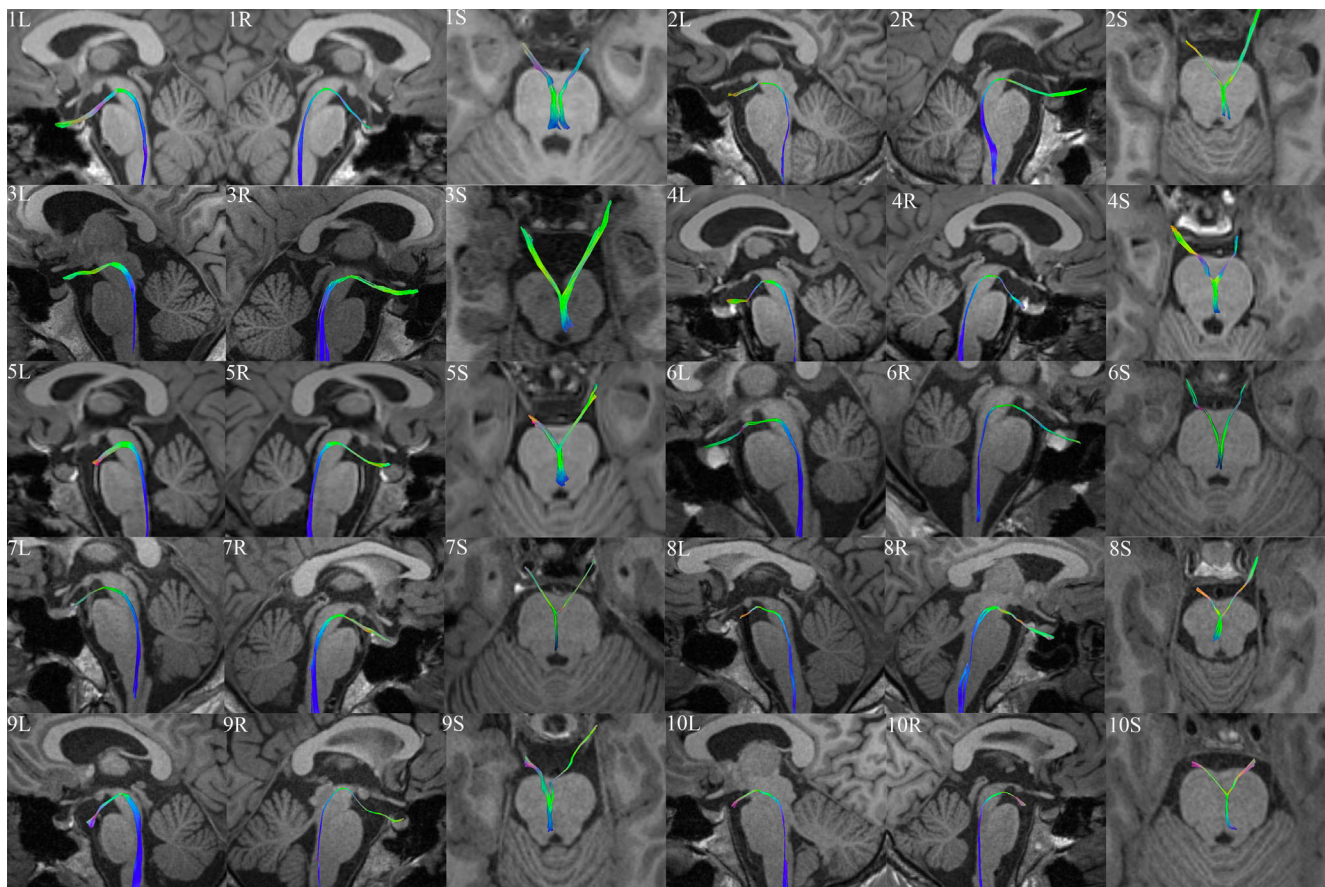
FIGURE 4 Fiber tracking in 10 healthy controls subjects, showing the lateral view of the left MLF, lateral view of the right MLF and superior view of the left and right MLF. The MLF was reconstructed in 37 cases (left and right). The MLF was not found on the left side of subject 15 and the right side of subjects 8 and 20. L, left; R, right; S, superior

of the MLF reconstructed from the diffusion images corresponded well with the histological anatomy. The MLF traveled ventral to the fourth ventricle floor and lateral to the median sulcus in the pons and medulla. Then, it ascended ventrolateral to the cerebral aqueduct and dorsal to the decussation of superior cerebellum peduncle in the midbrain. After that, it was in conjunction with the mesencephalic part of the oculomotor nerve at the rostral midbrain, which was the area that the mesencephalic part of the oculomotor nerve passed through the MLF. Furthermore, the left visualized MLF from the diffusion images originated from the vestibular nucleus and the abducens nucleus, which come together and ascended to connect with the oculomotor nucleus (Figure 6).

5 | DISCUSSION

In this study, we investigated the trajectory of the MLF with tractography in the HCP-1065 template, MGH healthy subjects and Xuanwu healthy controls and validated in the Duke CIVM brainstem 200 μm template. Tractography showed that the MLF traveled ventral to the fourth ventricle floor and lateral to the median sulcus in the pons and medulla. Then, it ascended ventrolateral to the cerebral

aqueduct and dorsal to the decussation of the superior cerebellum peduncle in the midbrain. After that, it was in conjunction with the mesencephalic part of the oculomotor nerve at the rostral midbrain. Furthermore, the reconstructed MLF in the Duke CIVM brainstem 200 μm template had the same trajectory with the MLF in the histological anatomy. This reconstruction also corresponded well with the previous findings (Meola et al., 2016; Miller, Mark, Ho, & Haughton, 1997; Yagmurlu et al., 2014; Yeo et al., 2020; Yoshino et al., 2016). At the same time, the changes of MLF resulting from BCM was evaluated for the first time through qualitative and quantitative analysis in BCM patients, and all 6 BCM patients showed displacement, which could cause eye movement dysfunction. Moreover, decreased QA, RDI and FA were observed in the MLF of lesion side when compared to the contralateral side, implying disruption in the MLF of lesion side. The alterations of QA, RDI and FA reflected the changes of MLF caused by BCM. This tractography protocol in our study did well in the reconstruction and evaluation of MLF.

The MLF consisted of ascending and descending fiber tracts, which mainly originated from the vestibular nucleus and nucleus of extraocular muscles (nucleus of oculomotor nerve, nucleus of trochlear nerve and nucleus of abducens nerve). The descending fiber

TABLE 2 The index of the MLF in the MGH diffusion data

		QA	RDI	FA	MD	AD
Subject 1	L	3.79059	7.44187	0.131012	0.260555	0.296708
	R	3.71871	7.43253	0.125566	0.265419	0.30045
Subject 2	L	3.70549	8.11377	0.128276	0.267147	0.301408
	R	3.91136	8.39721	0.122687	0.277597	0.312287
Subject 3	L	2.91931	7.23878	0.123542	0.226554	0.254588
	R	2.73811	7.27393	0.103336	0.243429	0.268259
Subject 4	L	2.95481	6.64684	0.135275	0.231435	0.264076
	R	2.64949	6.77148	0.0979567	0.260235	0.28446
Subject 5	L	3.84469	7.71322	0.157635	0.245684	0.285654
	R	3.78447	7.58396	0.148139	0.252679	0.291919
Subject 6	L	3.25747	6.09767	0.151353	0.24055	0.28012
	R	3.27027	5.95283	0.149769	0.247495	0.286905
Subject 7	L	2.7622	6.54714	0.128281	0.223773	0.253025
	R	2.7403	6.47073	0.127004	0.226436	0.256024
Subject 8	L	2.59291	6.25139	0.1237	0.230087	0.259138
	R	2.37523	6.05465	0.10996	0.236654	0.262666
Subject 9	L	2.27159	5.57954	0.0958217	0.267726	0.293108
	R	1.90837	5.53745	0.0870733	0.263524	0.284658
Subject 10	L	3.7378	7.60217	0.14447	0.2531	0.291443
	R	4.13723	7.783	0.154878	0.258314	0.300598
Subject 11	L	3.04806	6.18018	0.150001	0.230013	0.266562
	R	3.03889	6.18831	0.154646	0.225982	0.263084
Subject 12	L	2.76444	5.95361	0.136983	0.253968	0.290587
	R	2.59622	5.76771	0.124589	0.262021	0.296012
Subject 13	L	3.08427	6.69682	0.139318	0.227211	0.260325
	R	3.2165	6.7914	0.140762	0.227118	0.260851
Subject 14	L	2.7972	7.22929	0.100013	0.244522	0.269303
	R	2.9745	7.32713	0.110705	0.242875	0.269771
Subject 15	L	/	/	/	/	/
	R	3.2062	6.61294	0.137134	0.24769	0.283086
Subject 16	L	2.95261	6.29537	0.132928	0.233693	0.266546
	R	2.95862	6.30994	0.138349	0.229552	0.263208
Subject 17	L	3.54064	6.73409	0.145327	0.258289	0.298353
	R	3.76986	6.87761	0.14928	0.267174	0.309772
Subject 18	L	2.36565	5.72831	0.141574	0.209429	0.239713
	R	1.97227	5.32786	0.106296	0.234875	0.259929
Subject 19	L	4.5213	7.42927	0.189001	0.236509	0.286053
	R	4.64285	7.32749	0.178972	0.257486	0.307922
Subject 20	L	0.026364	0.0627276	0.128751	0.24032	0.271815
	R	0.0271075	0.0633629	0.145353	0.229144	0.26258
Subject 21	L	4.09964	7.85465	0.163053	0.236446	0.277088
	R	3.20572	7.27229	0.114765	0.268478	0.300075
Subject 22	L	3.05906	6.24403	0.131797	0.26196	0.298095
	R	3.48207	6.58111	0.15321	0.248684	0.289819
Subject 23	L	3.22713	6.50006	0.141717	0.250242	0.287218
	R	2.68426	6.18983	0.10368	0.272376	0.301736

TABLE 2 (Continued)

		QA	RDI	FA	MD	AD
Subject 24	L	2.55612	6.26944	0.119521	0.255758	0.28576
	R	2.04109	5.84338	0.0886301	0.283809	0.306923
Subject 25	L	1.9537	4.75272	0.120931	0.226432	0.253783
	R	1.63898	4.66951	0.0939714	0.245969	0.267287
Subject 26	L	2.42116	6.97505	0.0982473	0.278429	0.304144
	R	2.17923	6.19286	0.0956744	0.263812	0.286558
Subject 27	L	2.65509	6.02357	0.116447	0.239458	0.268691
	R	2.61976	6.1597	0.112852	0.252676	0.281492
Subject 28	L	3.69578	7.41283	0.147758	0.246221	0.284752
	R	3.69169	7.43229	0.144364	0.251889	0.290241
Subject 29	L	2.06153	4.58295	0.128668	0.237502	0.268595
	R	2.12689	4.61336	0.142239	0.229568	0.263094
Subject 30	L	2.97544	5.93868	0.136435	0.245993	0.281592
	R	3.06095	6.05056	0.140492	0.246758	0.284142
Subject 31	L	2.72768	5.70892	0.149998	0.22712	0.262018
	R	2.6052	5.70034	0.13405	0.240873	0.273436
Subject 32	L	2.3145	6.47756	0.100792	0.273486	0.298588
	R	3.17695	7.24963	0.150636	0.243774	0.281529
Subject 33	L	3.06622	6.46347	0.12818	0.254431	0.288606
	R	3.13972	6.4729	0.150421	0.239237	0.276648
Subject 34	L	2.45582	5.78516	0.116086	0.231894	0.259568
	R	2.38941	5.70518	0.120568	0.220988	0.249178
Subject 35	L	3.33897	7.65159	0.12441	0.245104	0.276916
	R	3.27781	7.66859	0.128139	0.246736	0.279353

Note: /, the MLF was not reconstructed.
Abbreviations: L, left; R, right.

tracts, mostly originating from the medial and inferior vestibular nucleus and known as the medial vestibulospinal tract, descend bilaterally to the motor neurons in the cervical spinal cord and innervate the neck muscles to form part of the reflex circuits by which the position and movements of the head are coordinated with the eyes. Other descending fiber tracts arise from the interstitial nucleus of Cajal and descend to the spinal cord to constitute the small interstitiospinal component of the MLF. The ascending fiber tracts, mainly originating from all four vestibular nucleus (superior, inferior, lateral and medial vestibular nucleus), constitute the vestibulomesencephalic projections and ascend bilaterally to the nucleus of the extraocular muscles, the interstitial nucleus of Cajal and the rostral interstitial nucleus of the MLF. There are also ascending fiber tracts originating from the internuclear neurons of the abducens nucleus, which ascend in the contralateral MLF to the oculomotor nucleus after crossing the midline and selectively excited motoneurons of the contralateral medial rectus muscle (Nieuwenhuys et al., 1988). These subcomponents of MLF have rarely been determined in tractography studies due to the lack of a precise definition of the corresponding nucleus in the structural and diffusional images. In our study, the subcomponents of MLF originated from the vestibular nucleus and the nucleus of the abducens

was visualized for the first time in the Duke CIVM brainstem 200 μm template. However, the decussated ascending and descending MLF fiber tracts, which crossed the midline and traveled in the contralateral MLF, were not reconstructed in the Duke CIVM brainstem 200 μm template. This may be constrained by the deterministic tracking algorithm or reconstruction models. Different tracking algorithms and reconstruction models should be used to visualize these decussated MLF fiber tracts. The probabilistic fiber tracking method, which has been applied successfully to reconstruct the fiber tracts of the brainstem and cerebellum, could be a potential way to track the decussated MLF fiber tracts if the deterministic algorithm cannot visualize these fiber bundles (Tang, Sun, Toga, Ringman, & Shi, 2018; van Baarsen et al., 2016).

Several advanced diffusion tractography studies have reconstructed the MLF (Meola et al., 2016; Yoshino et al., 2016). However, only one DTI study has visualized the MLF in the healthy controls with one ROI placed at the area of the interstitial nucleus of Cajal and one ROI placed on the ipsilateral MLF at the level of medulla (Yeo et al., 2020). The visualized MLF, which originated from the midbrain, descended through the posterior side of the medial lemniscus and terminated on the MLF of medulla on the posterior side of the

TABLE 3 The index of the MLF in the volunteer diffusion data

		QA	RDI	FA	MD	AD
Subject 1	L	0.0542941	0.191972	0.118862	0.199409	0.226468
	R	0.0549986	0.196657	0.13213	0.194422	0.225158
Subject 2	L	0.0860568	0.229214	0.178542	0.217822	0.261292
	R	0.0553924	0.167043	0.127657	0.149582	0.177568
Subject 3	L	0.0424461	0.147773	0.111574	0.121684	0.14195
	R	0.0524112	0.163471	0.129797	0.131065	0.154863
Subject 4	L	0.0185347	0.0698719	0.0633615	0.0574798	0.0680513
	R	0.0150879	0.0629673	0.0363229	0.0680211	0.0748305
Subject 5	L	0.131209	0.581533	0.17243	0.129263	0.150697
	R	0.144657	0.592188	0.1819	0.142796	0.170181
Subject 6	L	0.0886281	0.424365	0.162992	0.147336	0.16957
	R	0.0824716	0.41369	0.16283	0.144077	0.163767
Subject 7	L	0.0914946	0.419145	0.137233	0.153433	0.173702
	R	0.0983146	0.429349	0.141159	0.166307	0.188614
Subject 8	L	0.130725	0.581115	0.157197	0.150242	0.173482
	R	/	/	/	/	/
Subject 9	L	0.0754763	0.421819	0.118828	0.157166	0.174219
	R	0.0872907	0.439162	0.149746	0.141535	0.160846
Subject 10	L	0.0862065	0.404095	0.154669	0.137587	0.158813
	R	0.0983108	0.406337	0.152876	0.162878	0.189184
Subject 11	L	0.131394	0.194788	0.429322	0.672723	0.989325
	R	0.134141	0.191069	0.470267	0.607207	0.938634
Subject 12	L	0.079269	0.11702	0.422142	0.632285	0.917891
	R	0.0734764	0.106541	0.43012	0.629914	0.919561
Subject 13	L	0.0570765	0.0820393	0.258463	0.253651	0.407163
	R	0.0581265	0.084145	0.260243	0.243762	0.395146
Subject 14	L	0.119221	0.177344	0.45398	0.443474	0.694778
	R	0.106253	0.170166	0.411331	0.470673	0.697129
Subject 15	L	/	/	/	/	/
	R	0.156095	0.231354	0.414539	0.483401	0.717456
Subject 16	L	0.186305	0.302347	0.361023	0.490582	0.682791
	R	0.168614	0.287047	0.335528	0.492722	0.665221
Subject 17	L	0.188093	0.323173	0.320651	0.491991	0.661447
	R	0.187579	0.31701	0.333324	0.488601	0.661724
Subject 18	L	0.228356	0.370801	0.346853	0.515712	0.712536
	R	0.202676	0.345196	0.306526	0.551917	0.72666
Subject 19	L	0.123558	0.201638	0.313444	0.52086	0.691279
	R	0.132142	0.222971	0.3137	0.541732	0.714461
Subject 20	L	0.0759382	0.122102	0.37895	0.706635	0.981863
	R	/	/	/	/	/

Note: /, the MLF was not reconstructed.
Abbreviations: L, left; R, right.

medial lemniscus in the midline, was in line with our findings. However, the ability of DTI fiber tractography in the identification of MLF injury in BCM patients needs to be verified in the further study. In addition, the decussated MLF fibers, which crossed the midline and ascended in the contralateral MLF after originating from the vestibular nucleus and abducens nucleus, were not reconstructed. Furthermore, the subcomponents of the MLF fibers were not visualized in the DTI tractography, a higher angular resolution was suggested to localize
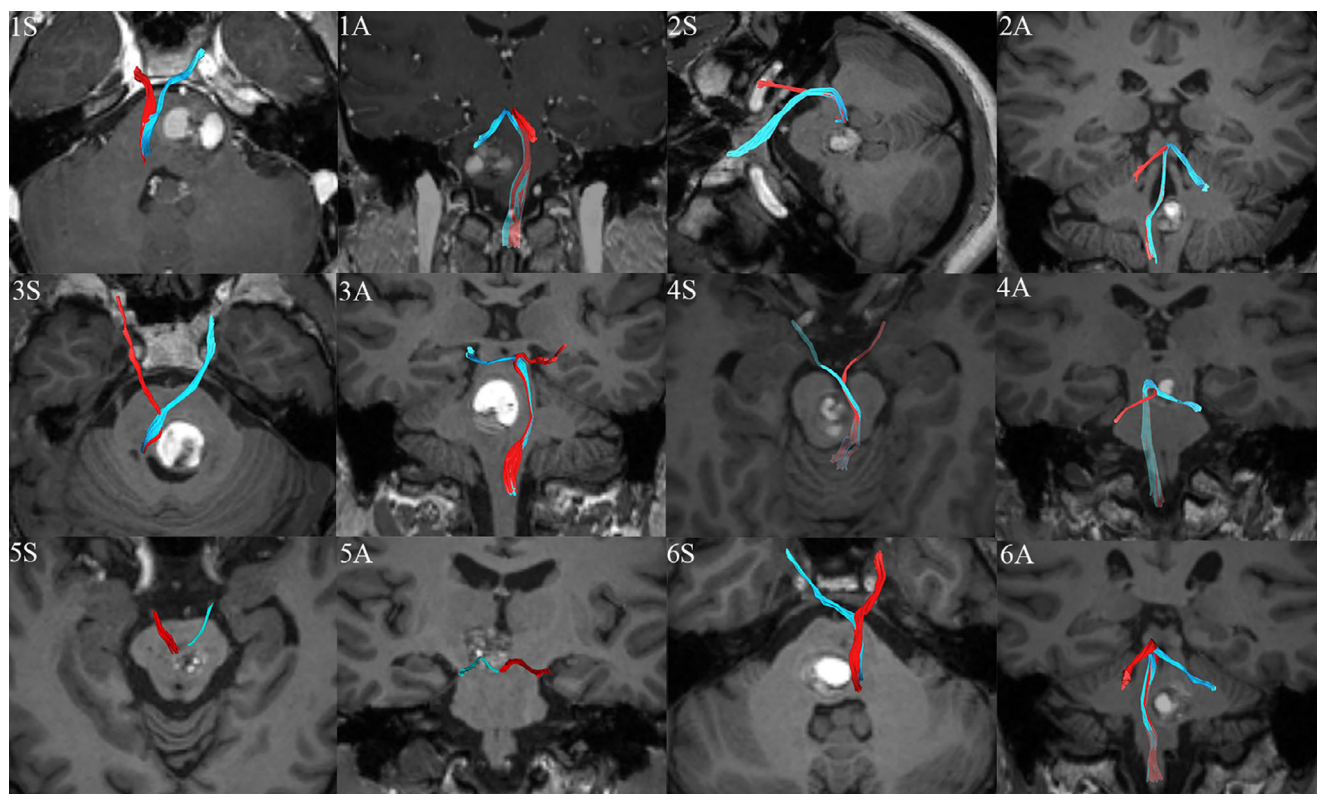
FIGURE 5 Fiber tracking in 6 BCM patients, showing the MLF from the superior view and anterior view. The MLF of the lesion side was blue and the MLF of contralateral side was red. In Patient 1, both of the right and left MLF were displaced by the BCM and the right MLF was squeezed to the left side (1S, 1A of this figure), this patient had numbness in the left limb but eye movement dysfunction. In Patient 2, both of the right and left MLF were displaced by the BCM and the left MLF was squeezed to the right side, this patient had left facial paralysis but eye movement dysfunction (2S, 2A of this figure). In Patient 3, both of the right and left MLF were displaced by the BCM and the right MLF was squeezed to the left side (3S, 3A of this figure), this patient had numbness in the left limb combined with horizontal nystagmus. In Patient 4, both of the right and left MLF were displaced by the BCM and the left MLF was squeezed to the right side (4S, 4A of this figure), this patient had adduction dysfunction of the left eye. In Patient 5, both of the right and left MLF were displaced by the BCM and the MLF was squeezed inferiorly (5S, 5A of this figure), this patient had ghosting combined with elevating dysfunction in both eyes. In Patient 6, both of the right and left MLF were displaced by the BCM and the left MLF was squeezed to the right side (6S, 6A of this figure), this patient had abduction dysfunction of the left eye combined with numbness of right limb. A, anterior; S, superior

and define the vestibular nucleus and nucleus of extraocular muscles (Sakaie et al., 2011), which would be helpful to determine the sub-components of the MLF.

Most DTI studies focused on the MLF injury caused by the multiple sclerosis. Decreased FA and increased MD and AD in the MLF were found to correlate with eye movement dysfunction in previous studies (Fox et al., 2008; McNulty et al., 2016; Sakaie et al., 2016). These studies concluded that DTI could find small MLF pathway lesions in the medulla, pons and midbrain. Compared to these studies, the changes of MLF caused by BCM were investigated for the first time through qualitative and quantitative analysis in our study. Qualitative analysis was used to evaluate the displacement and/or disruption of the MLF caused by the BCM. Quantitative analysis was used to identify MLF injury through the changes in DTI and GQI metrics. FA is good at evaluating the integrity of fiber pathways, while QA measures the spin density of anisotropy diffusion along a fiber pathway, which quantifies the quantity of diffusion water in each fiber

population (Yeh et al., 2016). In our cases, the qualitative result accurately visualized the orientation of the MLF in the lesion side, which was displaced to the contralateral side, and the surgical trajectory was selected based on the reconstruction of MLF. This visualization of MLF would improve the patients' neurological status after surgery. At the same time, the quantitative analysis found decreased QA and RDI in the MLF of lesion side when compared to the contralateral side, which indicated decreased spin density of anisotropy diffusion in the MLF resulting from the displacement. Moreover, the FA in the MLF of lesion side showed a significant decrease from the contralateral side, implying the reduction integrity in the MLF of lesion side. The decreased QA, combined with the decreased FA, indicated neuronal changes in the MLF of lesion side, which may be axonal loss and/or edema caused by the squeeze from BCM (Yeh et al., 2016). This substantial change could cause eye movement dysfunction in BCM patients. Horizontal nystagmus, adduction dysfunction and elevation dysfunction were identified in patients 3, 4 and 5, respectively,

TABLE 4   The index of the MLF in the brainstem CM diffusion data

Subject	Side	QA	RDI	FA	MD	AD
Patient 1	Lesion	0.0539457	0.0771502	0.392231	1.29967	1.78493
	Contra	0.0609724	0.0846525	0.43561	1.13057	1.63998
	Percentage of change	11.5%	8.9%	10.0%	15.0%	8.8
Patient 2	Lesion	0.0441388	0.0790086	0.244964	1.9855	2.43439
	Contra	0.0499292	0.0915013	0.260772	1.9754	2.42705
	Percentage of decrease	11.6%	13.7%	6.1%	0.51%	0.30%
Patient 3	Lesion	0.0608404	0.0868087	0.402746	1.44107	1.97297
	Contra	0.0629395	0.0925891	0.42774	1.32818	1.85169
	Percentage of decrease	3.3%	6.2%	5.8%	8.5%	6.5%
Patient 4	Lesion	0.0691138	0.117663	0.364035	1.59309	2.05367
	Contra	0.0691198	0.120213	0.359183	1.48198	1.92368
	Percentage of decrease	0.0087%	2.1%	1.4%	7.5%	6.8%
Patient 5	Lesion	0.0792102	0.0819547	0.347677	1.76487	2.39288
	Contra	0.0834673	0.0825679	0.400587	1.77767	2.46298
	Percentage of decrease	5.1%	0.74%	13.2%	0.72%	2.8%
Patient 6	Lesion	0.065284	0.0849069	0.400952	1.63779	2.191
	Contra	0.0715168	0.0933816	0.433152	1.3069	1.82254
	Percentage of decrease	8.7%	9.1%	7.4%	25.3%	20.2%

Abbreviation: Contra, contralateral.

TABLE 5   The mean value of index in the MLF

		QA	RDI	FA	MD	AD
MGH	L	2.92 ± 0.78	6.35 ± 1.39	0.13 ± 0.02	0.24 ± 0.02	0.27 ± 0.02
	R	2.88 ± 0.84	6.33 ± 1.39	0.12 ± 0.02	0.24 ± 0.02	0.28 ± 0.02
Health control	L	0.10 ± 0.05	0.28 ± 0.15	0.24 ± 0.12	0.32 ± 0.21	0.44 ± 0.32
	R	0.10 ± 0.05	0.26 ± 0.14	0.24 ± 0.13	0.32 ± 0.20	0.44 ± 0.30
BCM patients	Lesion	0.062 ± 0.012	0.088 ± 0.015	0.36 ± 0.060	1.62 ± 0.24	2.14 ± 0.25
	Contra	0.066 ± 0.011	0.094 ± 0.014	0.39 ± 0.068	1.50 ± 0.32	2.02 ± 0.34
P(MGH)	Paired-sample t-test	0.330	0.473	0.180	**0.046**	**0.029**
P(health control)	Paired-sample t-test	0.521	0.440	0.653	0.898	0.619
P(BCM patients)	Paired-sample t-test	**0.012**	**0.016**	**0.022**	0.063	0.113

Note: Bold values denote a significant difference observed in the QA (p = .012), RDI (p = .016), and FA (p = .022) between the lesion side and contralateral side, the QA (decreased 0.0087–11.6%), RDI (decreased 0.74–13.7%) and FA (decreased 1.4–13.2%) value on the lesion side was lower than that on the contralateral side, implying that the MLF of lesion side may have disruption. A significant difference was observed in the MD (p = .046) and AD (p = .029) between the left and right side in the MGH subjects, while there is no significance in the MD (p = .898) and AD (p = .619) value between the left and right side in the HCP subjects, implied that the MD and AD value may be not suitable for the reflection of the changes of MLF, it should be evaluated in more subjects.
Abbreviations: Contra, contralateral; L, left; R, right.

indicated axonal loss of the MLF displaced by the BCM. On the other hand, eye movement dysfunction was not found in patients 1 and 2, implying edema of the MLF resulted from BCM.

The qualitative analysis and quantitative analysis based on GQI have been used to define the relationship between the corticospinal tract and BCM in previous study, which found that the disruption of corticospinal tract corresponded with an obvious decrease percentage of QA value (Faraji et al., 2015). In our study, the displaced MLF,

combined with the decreased QA, RDI and FA, was identified in BCM patients, while the decrease percentage of QA (0.0087–11.6%), RDI (0.74–13.7%) and FA (1.4–13.2%) was low in all six patients, which may lead to an indiscernible disruption of MLF in the lesion side. Meanwhile, the low decrease percentage of QA, RDI and FA value indicated that the eye movement dysfunction maybe reversible, which should be evaluated in the further longitudinal analysis. Compared to the previous studies, the segmentation of perilesional MLF was not

TABLE 6 The demographics and clinical manifestations of the BCM patients

Patient	Sex	Age	BCM position	Clinical manifestation
1	F	37	Right pons	Numbness of left limb
2	F	27	Left pons	Left facial paralysis
3	M	42	Right pons	Horizontal nystagmus and numbness of left limb
4	M	41	Left midbrain	Adduction dysfunction of the left eye
5	F	53	Right midbrain	Ghosting and elevating dysfunction in both eyes
6	F	58	Left pons	Abduction dysfunction of the left eye and numbness of right limb

Abbreviations: F, female; M, male.
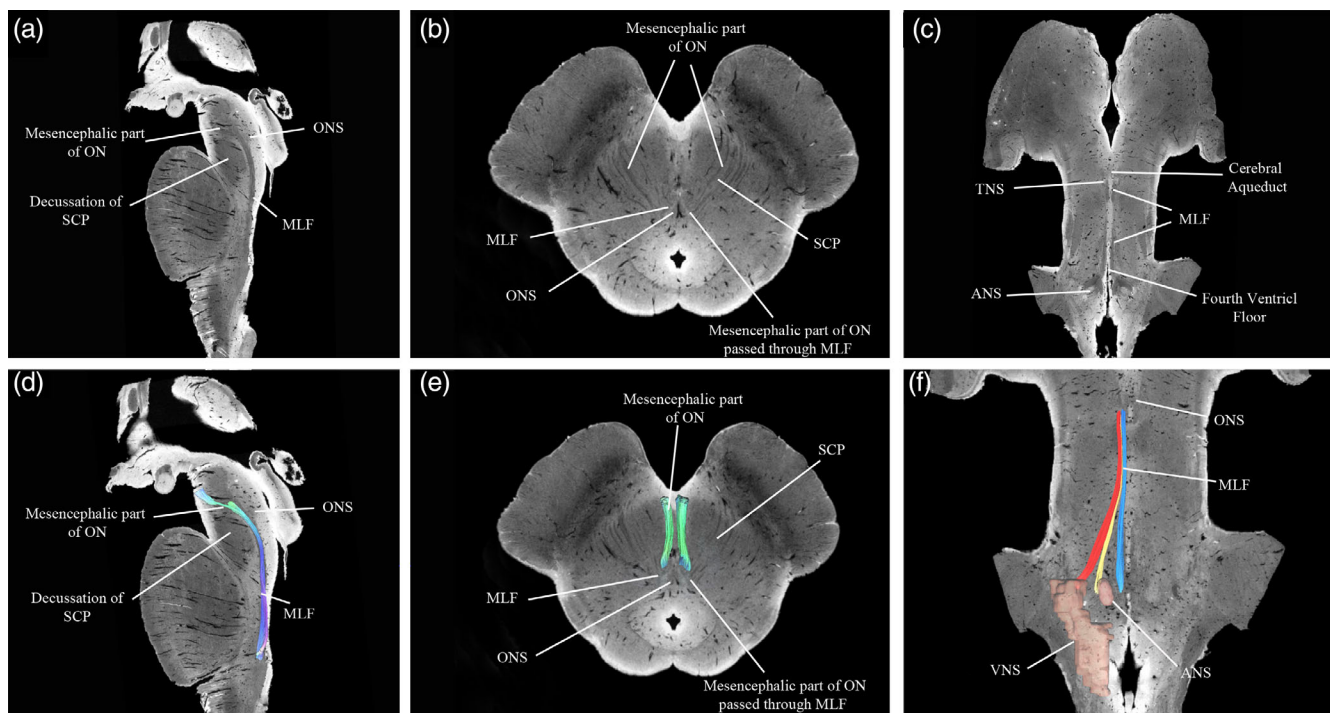
FIGURE 6 Fiber tracking in Duke CIVM 200 μm template. (a) The left sagittal image of the specimen near the median sulcus level, the MLF traveled ventral to the fourth ventricle floor and lateral to the median sulcus in the pons and medulla. Then, it ascended ventrolateral to the cerebral aqueduct and dorsal to the decussation of superior cerebellum peduncle in the midbrain. After that, it was in conjunction with the mesencephalic part of the oculomotor nerve at the rostral midbrain. (b) The superior axial image of the specimen at the superior colliculus level, the MLF was located ventrolateral to the oculomotor nucleus, the mesencephalic part of oculomotor nerve went in to the superior cerebellum peduncle after passing through the MLF. (c) The posterior coronal image of the specimen anterior to the cerebral aqueduct level, the MLF traveled ventral to the fourth ventricle floor and lateral to the median sulcus in the pons and medulla. Then, it ascended ventrolateral to the cerebral aqueduct. (d) The MLF reconstructed from the diffusion images had the same trajectory with the MLF in the histological anatomy in (a). (e) The MLF reconstructed from the diffusion images was in conjunction with the mesencephalic part of the oculomotor nerve at the rostral midbrain, which was the area that the mesencephalic part of the oculomotor nerve passed through the MLF. (f) The left MLF reconstructed from the diffusion images originated from the vestibular nucleus and abducens nucleus and ascended to connect with the oculomotor nucleus. ANS, abducens nucleus; ON, oculomotor nerve; ONS, oculomotor nucleus; SCP, superior cerebellum peduncle; TNS, trochlear nucleus; VNS, vestibular nucleus

performed in this work since that the MLF in the lesion side and contralateral side were both displaced by the BCM in all six patients, which resulted from the adjacency between the left and right MLF.

In addition, the anatomical relationship between the MLF and oculomotor nerve was investigated in our study. The rostral part of the MLF was found in conjunction with the mesencephalic part of the oculomotor nerve near the oculomotor nucleus complex in the

tractography. In fact, the mesencephalic part of the oculomotor nerve passed through the MLF after originating from the oculomotor nucleus and was divided into caudal fascicles, intermediate fascicles and rostral fascicles according to their course from the MLF to the interpeduncular cistern (Vitošević et al., 2013). After that, these fascicles passed through or medial to the red nucleus as discrete serpiginous bands and exited the midbrain between the cerebral

peduncles (Miller et al., 1997). The conjunction between the MLF and the mesencephalic part of the oculomotor nerve at the rostral midbrain in the tractography corresponded well these histological studies, which was the area that the mesencephalic part of the oculomotor nerve passed through the MLF. The mesencephalic part of the oculomotor nerve tracked in our work extended media to the superior cerebellum peduncle and red nucleus, while the mesencephalic part of the oculomotor nerve passed through the superior cerebellum peduncle and red nucleus was not visualized. We are now trying to reconstruct the mesencephalic part of the oculomotor nerve passed through the red nucleus using fiber cluster, an automatic fiber tract reconstruction methods that assembles fibers with similar trajectories into clusters according to their fiber geometry (Maddah, Grimson, Warfield, & Wells, 2008; O'Donnell & Westin, 2007), which has been reported to segment or cluster whole-brain tractography automatically across subjects (O'Donnell et al., 2017; Wu et al., 2018; Zhang et al., 2018).

Several limitations existed in our study: (1) The MLF traveled to the interstitial nucleus of Cajal and rostral interstitial nucleus of the MLF is not visualized in our work. The interstitial nucleus of Cajal and rostral interstitial nucleus of the MLF are located superior and anterior to the oculomotor nucleus, it is hard to differential these two nucleus from the oculomotor nucleus, and the MLF reconstructed in our work mostly traveled to the oculomotor nucleus and trochlear nucleus. At the same time, the subcomponents of the MLF were not tracked in the subject-specific and template tractography, though the subcomponents of MLF originated from the vestibular nucleus and the abducens nucleus were visualized in the Duke CIVM brainstem 200 μm template. (2) The preoperative changes in MLF were investigated in our study, and further longitudinal analysis needs to be implemented to evaluate changes in the MLF after surgery. MLF alterations should be monitored at multiple time points if possible, including at 3 months, 6 months, 1 year and 2 years after surgery. It is necessary to evaluate the injury and/or repair of MLF in a dynamic process. (3) Limited by the number of BMC patients in this study, obvious MLF disruption was not observed in the included BCM patients. Furthermore, the correlation between the metrics of DTI and GQI in the MLF and the corresponding clinical manifestations should be further evaluated in studies with large samples.

6 | CONCLUSION

This study investigated the trajectory of MLF and explored its anatomical relationship with the mesencephalic part of the oculomotor nerve through tractography technique. The MLF was visualized accurately with our protocol using GQI based fiber tracking. Furthermore, the alterations of MLF caused by the BCM were reflected using qualitative analysis and quantitative analysis. This tractography protocol is an important tool in the reconstruction and evaluation of the MLF.

ORCID

Mengjun Li https://orcid.org/0000-0003-1674-9369
Qingrun Zeng https://orcid.org/0000-0001-6485-8178

REFERENCES

Adil, S. M., Calabrese, E., Charalambous, L. T., Cook, J. J., Rahimpour, S., Atik, A. F., ... White, L. E. (2021). A high-resolution interactive atlas of the human brainstem using magnetic resonance imaging. *NeuroImage*, *237*, 118135. https://doi.org/10.1016/j.neuroimage.2021.118135

Bae, Y. J., Kim, J. H., Choi, B. S., Jung, C., & Kim, E. (2013). Brainstem pathways for horizontal eye movement: Pathologic correlation with MR imaging. *Radiographics*, *33*(1), 47–59. https://doi.org/10.1148/rg.331125033

Calabrese, E., Hickey, P., Hulette, C., Zhang, J., Parente, B., Lad, S. P., & Johnson, G. A. (2015). Postmortem diffusion MRI of the human brainstem and thalamus for deep brain stimulator electrode localization. *Human Brain Mapping*, *36*(8), 3167–3178. https://doi.org/10.1002/hbm.22836

Celtikci, P., Fernandes-Cabral, D. T., Yeh, F. C., Panesar, S. S., & Fernandez-Miranda, J. C. (2018). Generalized q-sampling imaging fiber tractography reveals displacement and infiltration of fiber tracts in low-grade gliomas. *Neuroradiology*, *60*(3), 267–280. https://doi.org/10.1007/s00234-018-1985-5

Faraji, A. H., Abhinav, K., Jarbo, K., Yeh, F. C., Shin, S. S., Pathak, S., ... Friedlander, R. M. (2015). Longitudinal evaluation of corticospinal tract in patients with resected brainstem cavernous malformations using high-definition fiber tractography and diffusion connectometry analysis: Preliminary experience. *Journal of Neurosurgery*, *123*(5), 1133–1144. https://doi.org/10.3171/2014.12.jns142169

Fernandez-Miranda, J. C., Pathak, S., Engh, J., Jarbo, K., Verstynen, T., Yeh, F.-C., ... Friedlander, R. (2012). High-definition fiber tractography of the human brain. *Neurosurgery*, *71*(2), 430–453. https://doi.org/10.1227/NEU.0b013e3182592faa

Fernández-Miranda, J. C., Wang, Y., Pathak, S., Stefaneau, L., Verstynen, T., & Yeh, F. C. (2015). Asymmetry, connectivity, and segmentation of the arcuate fascicle in the human brain. *Brain Structure & Function*, 220(3), 1665–1680.

Fiester, P., Baig, S. A., Patel, J., & Rao, D. (2020). An anatomic, imaging, and clinical review of the medial longitudinal fasciculus. *Journal of Clinical Imaging Science*, 10, 83. https://doi.org/10.25259/jcis_49_2020

Fox, R. J., McColl, R. W., Lee, J. C., Frohman, T., Sakaie, K., & Frohman, E. (2008). A preliminary validation study of diffusion tensor imaging as a measure of functional brain injury. *Archives of Neurology*, 65(9), 1179–1184. https://doi.org/10.1001/archneur.65.9.1179

Frohman, T. C., Galetta, S., Fox, R., Solomon, D., Straumann, D., Filippi, M., … Frohman, E. M. (2008). Pearls & oy-sters: The medial longitudinal fasciculus in ocular motor physiology. *Neurology*, 70(17), e57–e67. https://doi.org/10.1212/01.wnl.0000310640.37810.b3

Jenkinson, M., Beckmann, C. F., Behrens, T. E., Woolrich, M. W., & Smith, S. M. (2012). FSL. *Neuroimage*, 62(2), 782–790. https://doi.org/10.1016/j.neuroimage.2011.09.015

Li, M., Ribas, E. C., Wei, P., Li, M., Zhang, H., & Guo, Q. (2020). The ansa peduncularis in the human brain: A tractography and fiber dissection study. *Brain Research*, 1746, 146978. https://doi.org/10.1016/j.brainres.2020.146978

Maddah, M., Grimson, W. E., Warfield, S. K., & Wells, W. M. (2008). A unified framework for clustering and quantitative analysis of white matter fiber tracts. *Medical Image Analysis*, 12(2), 191–202. https://doi.org/10.1016/j.media.2007.10.003

Maierhein, K. H., Neher, P. F., Houde, J. C., Côté, M. A., Garyfallidis, E., Zhong, J., … Ji, Q. (2017). The challenge of mapping the human connectome based on diffusion tractography. *Nature Communications*, 8(1), 1349.

McNulty, J. P., Lonergan, R., Bannigan, J., O'Laoide, R., Rainford, L. A., & Tubridy, N. (2016). Visualisation of the medial longitudinal fasciculus using fibre tractography in multiple sclerosis patients with internuclear ophthalmoplegia. *Irish Journal of Medical Science*, 185(2), 393–402. https://doi.org/10.1007/s11845-016-1405-y

Meola, A., Yeh, F. C., Fellows-Mayle, W., Weed, J., & Fernandez-Miranda, J. C. (2016). Human connectome-based tractographic atlas of the brainstem connections and surgical approaches. *Neurosurgery*, 79(3), 437–455. https://doi.org/10.1227/neu.0000000000001224

Miller, M. J., Mark, L. P., Ho, K. C., & Haughton, V. M. (1997). Anatomic relationship of the oculomotor nuclear complex and medial longitudinal fasciculus in the midbrain. *AJNR. American Journal of Neuroradiology*, 18(1), 111–113.

Nieuwenhuys, R., Voogd, J., & van Huijzen, C. (1988). *The human central nervous system: A synopsis and atlas* (3rd revised edition ed.). Berlin: Springer-Verlag.

O'Donnell, L. J., Suter, Y., Rigolo, L., Kahali, P., Zhang, F., Norton, I., … Golby, A. J. (2017). Automated white matter fiber tract identification in patients with brain tumors. *Neuroimage Clinical*, 13, 138–153. https://doi.org/10.1016/j.nicl.2016.11.023

O'Donnell, L. J., & Westin, C. F. (2007). Automatic tractography segmentation using a high-dimensional white matter atlas. *IEEE Transactions on Medical Imaging*, 26(11), 1562–1575. https://doi.org/10.1109/tmi.2007.906785

Panesar, S. S., Belo, J. T. A., Yeh, F. C., & Fernandez-Miranda, J. C. (2019). Structure, asymmetry, and connectivity of the human temporo-parietal aslant and vertical occipital fasciculi. *Brain Structure & Function*, 224(2), 907–923. https://doi.org/10.1007/s00429-018-1812-0

Sakai, K., Yokota, H., Akazawa, K., & Yamada, K. (2014). Brainstem white matter tracts and the control of eye movements. *Seminars in Ultrasound, CT, and MR*, 35(5), 517–526. https://doi.org/10.1053/j.sult.2014.06.009

Sakaie, K., Takahashi, M., Dimitrov, I., Togao, O., Davis, S., Remington, G., … Frohman, E. (2011). Diffusion tensor imaging the medial longitudinal fasciculus in INO: Opportunities and challenges. *Annals of the New York Academy of Sciences*, 1233, 307–312. https://doi.org/10.1111/j.1749-6632.2011.06156.x

Sakaie, K., Takahashi, M., Remington, G., Wang, X., Conger, A., Conger, D., … Frohman, E. (2016). Correlating function and imaging measures of the medial longitudinal fasciculus. *PLoS One*, 11(1), e0147863. https://doi.org/10.1371/journal.pone.0147863

Tang, Y., Sun, W., Toga, A. W., Ringman, J. M., & Shi, Y. (2018). A probabilistic atlas of human brainstem pathways based on connectome imaging data. *NeuroImage*, 169, 227–239. https://doi.org/10.1016/j.neuroimage.2017.12.042

van Baarsen, K. M., Kleinnijenhuis, M., Jbabdi, S., Sotiropoulos, S. N., Grotenhuis, J. A., & van Cappellen van Walsum, A. M. (2016). A probabilistic atlas of the cerebellar white matter. *Neuroimage*, 124(Pt A), 724–732. https://doi.org/10.1016/j.neuroimage.2015.09.014

Vitošević, Z., Marinković, S., Cetković, M., Stimec, B., Todorović, V., Kanjuh, V., & Milisavljević, M. (2013). Intramesencephalic course of the oculomotor nerve fibers: Microanatomy and possible clinical significance. *Anatomical Science International*, 88(2), 70–82. https://doi.org/10.1007/s12565-012-0166-6

Wu, Y., Zhang, F., Makris, N., Ning, Y., Norton, I., She, S., … O'Donnell, L. J. (2018). Investigation into local white matter abnormality in emotional processing and sensorimotor areas using an automatically annotated fiber clustering in major depressive disorder. *NeuroImage*, 181, 16–29. https://doi.org/10.1016/j.neuroimage.2018.06.019

Yagmurlu, K., Rhoton, A. L., Jr., Tanriover, N., & Bennett, J. A. (2014). Three-dimensional microsurgical anatomy and the safe entry zones of the brainstem. *Neurosurgery*, 10(Suppl. 4), 602–619; discussion 619-620. https://doi.org/10.1227/neu.0000000000000466

Yeh, F. C., Panesar, S., Fernandes, D., Meola, A., Yoshino, M., Fernandez-Miranda, J. C., … Verstynen, T. (2018). Population-averaged atlas of the macroscale human structural connectome and its network topology. *NeuroImage*, 178, 57–68. https://doi.org/10.1016/j.neuroimage.2018.05.027

Yeh, F. C., & Tseng, W. Y. (2011). NTU-90: A high angular resolution brain atlas constructed by q-space diffeomorphic reconstruction. *NeuroImage*, 58(1), 91–99. https://doi.org/10.1016/j.neuroimage.2011.06.021

Yeh, F. C., Verstynen, T. D., Wang, Y., Fernández-Miranda, J. C., & Tseng, W. Y. (2013). Deterministic diffusion fiber tracking improved by quantitative anisotropy. *PLoS One*, 8(11), e80713. https://doi.org/10.1371/journal.pone.0080713

Yeh, F. C., Vettel, J. M., Singh, A., Poczos, B., Grafton, S. T., Erickson, K. I., … Verstynen, T. D. (2016). Quantifying differences and similarities in whole-brain white matter architecture using local connectome fingerprints. *PLoS Computational Biology*, 12(11), e1005203. https://doi.org/10.1371/journal.pcbi.1005203

Yeh, F. C., Wedeen, V. J., & Tseng, W. Y. (2010). Generalized q-sampling imaging. *IEEE Transactions on Medical Imaging*, 29(9), 1626–1635. https://doi.org/10.1109/tmi.2010.2045126

Yeo, S. S., Jang, S. H., Kwon, J. W., & Cho, I. H. (2020). Three-dimensional identification of the medial longitudinal fasciculus in the human brain: A diffusion tensor imaging study. *Journal of Clinical Medicine*, 9(5), 1340. https://doi.org/10.3390/jcm9051340

Yoshino, M., Abhinav, K., Yeh, F. C., Panesar, S., Fernandes, D., Pathak, S., … Fernandez-Miranda, J. C. (2016). Visualization of cranial nerves using high-definition fiber tractography. *Neurosurgery*, 79(1), 146–165. https://doi.org/10.1227/neu.0000000000001241

Zhang, F., Savadjiev, P., Cai, W., Song, Y., Rathi, Y., Tunc, B., … O'Donnell, L. J. (2018). Whole brain white matter connectivity

analysis using machine learning: An application to autism. *NeuroImage*, 172, 826–837. https://doi.org/10.1016/j.neuroimage.2017.10.029

Zhang, H., Wang, Y., Lu, T., Qiu, B., Tang, Y., Ou, S., … Wang, Y. (2013). Differences between generalized q-sampling imaging and diffusion tensor imaging in the preoperative visualization of the nerve fiber tracts within peritumoral edema in brain. *Neurosurgery*, 73(6), 1044–1053; discussion 1053. https://doi.org/10.1227/NEU.0000000000000146